LOSS FUNCTION IN A THREE LAYER SILICENE STRUCTURE AT ZERO TEMPERATURE

C. CARAIANI[1,a], L. ION[1,2]

[1]University of Bucharest, Faculty of Physics,
PO Box MG11, 077125, Măgurele-Bucharest, Romania
Corresponding author[a]: claudiu.caraiani@gmail.com
[2]Materials and Devices for Electronics and Optoelectronics Research Center,
PO Box MG11, 077125, Măgurele-Bucharest, Romania

Received June 21, 2024

Abstract. We compute theoretically the loss function in a three layer silicene structure within random phase approximation (RPA) at zero temperature in the homogeneous and inhomogeneous cases. We get analytical expressions for the loss function restricted to the acoustic and optical plasmon branches in the long wavelength approximation. Numerical computations show that as we increase the interlayer distance between the silicene layers the broadened peaks in the loss function associated with the damped plasmons start to merge. Another important effect that we observe numerically is that the plasmonic spectral weight of the loss function associated with undamped plasmonic branches is dominated by the acoustic plasmons.

Key words: Plasmons, Loss Function, Heterostructure, Silicene.

DOI: https://doi.org/10.59277/RomJPhys.2024.69.616

1. INTRODUCTION

Silicene is the silicon counterpart of graphene. It has two-dimensional A and B honeycomb sublattices like graphene but with an out of plane buckling. The A and B sublattices are arranged in two vertical planes separated by a distance d ≈ 0.46 Å [1, 2]. Unlike graphene, silicene exhibits a strong spin-orbit interaction which in conjunction with its buckled geometry induces a nonzero band gap, $2\Delta_{SO}$, in the energy spectrum. When an out-of-plane electric field E_z is applied the asymmetry between the two sublattices induces an onsite potential difference. This property makes the band gap of silicene tunable allowing one to distinguish between the different phases, topological insulator, valley-spin polarized metal and band insulator. Due to the fact that the bandgap is tunable, in comparison to graphene, it makes out of silicene a strong candidate for designing a field effect transistor that works at room temperature [3, 4].

It is well known that collective excitations are important properties of many-body systems. The physics of plasmonic oscillations in single and multilayer materials can have potential applications in plasmonics, photonics and optoelectronics [5–12]. Theoretical investigations on plasmons in monolayer silicene (MLS) [13–16], double

layer silicene (DLS) [17] and multilayer silicene systems [19] have been conducted at zero and finite temperature.

Up until now, to the best of our knowledge, the loss function in a three layer silicene (TLS) structure has not been investigated. We will define the loss function as $-\text{Im Tr}[\hat{\Pi}^R(\mathbf{q},\omega)]$ (the negative imaginary part of the trace of the retarded polarization matrix) [24, 25].

This paper is organized as follows. In Sec. 2 we describe the theoretical formalism. In Sec. 3 we present the numerical and analytical results of the calculations and discuss them in detail. Sec. 4 contains the main conclusions of the paper.

2. THEORY

We investigate a structure made of monolayer silicene deposited on dielectric substrates as shown in Fig. 1.

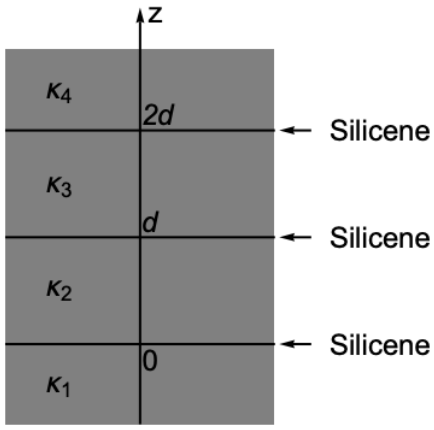

Fig. 1 – A three layer silicene (TLS) structure.

The Dyson equation of the retarded polarization matrix in the RPA approximation [26] for $\omega > 0$ is

$$\hat{\Pi}^R(\mathbf{q},\omega) = \hat{\Pi}^{0,R}(\mathbf{q},\omega) + \hat{\Pi}^{0,R}(\mathbf{q},\omega)\hat{V}(\mathbf{q})\hat{\Pi}^R(\mathbf{q},\omega) \tag{1}$$

where the zero-th order retarded polarization matrix is

$$\hat{\Pi}^{0,R}(\mathbf{q},\omega) = \begin{pmatrix} \Pi_1^0(\mathbf{q},\omega) & 0 & 0 \\ 0 & \Pi_2^0(\mathbf{q},\omega) & 0 \\ 0 & 0 & \Pi_3^0(\mathbf{q},\omega) \end{pmatrix} \tag{2}$$

and the Coulomb tensor

$$\hat{V}(\mathbf{q}) = \begin{pmatrix} \mathrm{v}_{11}(\mathbf{q}) & \mathrm{v}_{12}(\mathbf{q}) & \mathrm{v}_{13}(\mathbf{q}) \\ \mathrm{v}_{21}(\mathbf{q}) & \mathrm{v}_{22}(\mathbf{q}) & \mathrm{v}_{23}(\mathbf{q}) \\ \mathrm{v}_{31}(\mathbf{q}) & \mathrm{v}_{32}(\mathbf{q}) & \mathrm{v}_{33}(\mathbf{q}) \end{pmatrix} \tag{3}$$

Hence Eq. (1) becomes

$$\hat{\Pi}^R(\mathbf{q},\omega) = \frac{1}{\epsilon(\mathbf{q},\omega)} \begin{pmatrix} \hat{\Pi}^R_{11}(\mathbf{q},\omega) & \hat{\Pi}^R_{12}(\mathbf{q},\omega) & \hat{\Pi}^R_{13}(\mathbf{q},\omega) \\ \hat{\Pi}^R_{21}(\mathbf{q},\omega) & \hat{\Pi}^R_{22}(\mathbf{q},\omega) & \hat{\Pi}^R_{23}(\mathbf{q},\omega) \\ \hat{\Pi}^R_{31}(\mathbf{q},\omega) & \hat{\Pi}^R_{32}(\mathbf{q},\omega) & \hat{\Pi}^R_{33}(\mathbf{q},\omega) \end{pmatrix} \tag{4}$$

The matrix elements are given by

$$\hat{\Pi}^R_{11}(\mathbf{q},\omega) = \Pi^0_1(\mathbf{q},\omega)\epsilon_{23}(\mathbf{q},\omega) \tag{5a}$$

$$\hat{\Pi}^R_{12}(\mathbf{q},\omega) = \Pi^0_2(\mathbf{q},\omega)[\mathrm{v}_{12}(\mathbf{q})\Pi^0_1(\mathbf{q},\omega) + (\mathrm{v}_{13}(\mathbf{q})\mathrm{v}_{32}(\mathbf{q}) - \mathrm{v}_{12}(\mathbf{q})\mathrm{v}_{33}(\mathbf{q}))\Pi^0_1(\mathbf{q},\omega)\Pi^0_3(\mathbf{q},\omega)] \tag{5b}$$

$$\hat{\Pi}^R_{13}(\mathbf{q},\omega) = \Pi^0_3(\mathbf{q},\omega)[\mathrm{v}_{13}(\mathbf{q})\Pi^0_1(\mathbf{q},\omega) + (\mathrm{v}_{12}(\mathbf{q})\mathrm{v}_{23}(\mathbf{q}) - \mathrm{v}_{13}(\mathbf{q})\mathrm{v}_{22}(\mathbf{q}))\Pi^0_1(\mathbf{q},\omega)\Pi^0_2(\mathbf{q},\omega)] \tag{5c}$$

$$\hat{\Pi}^R_{21}(\mathbf{q},\omega) = \Pi^0_1(\mathbf{q},\omega)[\mathrm{v}_{21}(\mathbf{q})\Pi^0_2(\mathbf{q},\omega) + (\mathrm{v}_{23}(\mathbf{q})\mathrm{v}_{31}(\mathbf{q}) - \mathrm{v}_{21}(\mathbf{q})\mathrm{v}_{33}(\mathbf{q}))\Pi^0_2(\mathbf{q},\omega)\Pi^0_3(\mathbf{q},\omega)] \tag{5d}$$

$$\hat{\Pi}^R_{22}(\mathbf{q},\omega) = \Pi^0_2(\mathbf{q},\omega)\epsilon_{13}(\mathbf{q},\omega) \tag{5e}$$

$$\hat{\Pi}^R_{23}(\mathbf{q},\omega) = \Pi^0_3(\mathbf{q},\omega)[\mathrm{v}_{23}(\mathbf{q})\Pi^0_2(\mathbf{q},\omega) + (\mathrm{v}_{13}(\mathbf{q})\mathrm{v}_{21}(\mathbf{q}) - \mathrm{v}_{11}(\mathbf{q})\mathrm{v}_{23}(\mathbf{q}))\Pi^0_1(\mathbf{q},\omega)\Pi^0_2(\mathbf{q},\omega)] \tag{5f}$$

$$\hat{\Pi}^R_{31}(\mathbf{q},\omega) = \Pi^0_1(\mathbf{q},\omega)[\mathrm{v}_{31}(\mathbf{q})\Pi^0_3(\mathbf{q},\omega) + (\mathrm{v}_{21}(\mathbf{q})\mathrm{v}_{32}(\mathbf{q}) - \mathrm{v}_{22}(\mathbf{q})\mathrm{v}_{31}(\mathbf{q}))\Pi^0_2(\mathbf{q},\omega)\Pi^0_3(\mathbf{q},\omega)] \tag{5g}$$

$$\hat{\Pi}^R_{32}(\mathbf{q},\omega) = \Pi^0_2(\mathbf{q},\omega)[\mathrm{v}_{32}(\mathbf{q})\Pi^0_3(\mathbf{q},\omega) + (\mathrm{v}_{12}(\mathbf{q})\mathrm{v}_{31}(\mathbf{q}) - \mathrm{v}_{11}(\mathbf{q})\mathrm{v}_{32}(\mathbf{q}))\Pi^0_1(\mathbf{q},\omega)\Pi^0_3(\mathbf{q},\omega)] \tag{5h}$$

$$\hat{\Pi}^R_{33}(\mathbf{q},\omega) = \Pi^0_3(\mathbf{q},\omega)\epsilon_{12}(\mathbf{q},\omega) \tag{5i}$$

Here $\mathrm{v}_{ii}(\mathbf{q})$ and $\mathrm{v}_{ij}(\mathbf{q})$ are the intra- and inter-layer Coulomb matrix elements [21]

$$\mathrm{v}_{ij}(\mathbf{q}) = \frac{2\pi e^2}{q} f_{ij}(\mathbf{q}) \tag{6}$$

with

$$f_{11}(\mathbf{q}) = \frac{1}{4\pi\epsilon_0}\frac{2\left[(\kappa_2+\kappa_3)(\kappa_3-\kappa_4)+2\kappa_3(\kappa_2-\kappa_3)e^{2qd}+(\kappa_2+\kappa_3)(\kappa_3+\kappa_4)e^{4qd})\right]}{M(qd)} \tag{7a}$$

$$f_{22}(\mathbf{q}) = \frac{1}{4\pi\epsilon_0}\frac{8e^{2qd}\left[\kappa_1\cosh(qd)+\kappa_2\sinh(qd)\right]\left[\kappa_3\cosh(qd)+\kappa_4\sinh(qd)\right]}{M(qd)} \tag{7b}$$

$$f_{33}(\mathbf{q}) = \frac{1}{4\pi\epsilon_0}\frac{2\left[(\kappa_2+\kappa_3)(\kappa_2-\kappa_1)+2\kappa_2(\kappa_3-\kappa_2)e^{2qd}+(\kappa_1+\kappa_2)(\kappa_2+\kappa_3)e^{4qd})\right]}{M(qd)} \tag{7c}$$

$$f_{12}(\mathbf{q}) = f_{21}(\mathbf{q}) = \frac{1}{4\pi\epsilon_0}\frac{8\kappa_2 e^{2qd}\left[\kappa_3\cosh(qd)+\kappa_4\sinh(qd)\right]}{M(qd)} \tag{7d}$$

$$f_{13}(\mathbf{q}) = f_{31}(\mathbf{q}) = \frac{1}{4\pi\epsilon_0}\frac{8\kappa_2\kappa_3 e^{2qd}}{M(qd)} \tag{7e}$$

$$f_{32}(\mathbf{q}) = f_{23}(\mathbf{q}) = \frac{1}{4\pi\epsilon_0}\frac{8\kappa_3 e^{2qd}\left[\kappa_2\cosh(qd)+\kappa_1\sinh(qd)\right]}{M(qd)} \tag{7f}$$

$$M(qd) = (\kappa_1-\kappa_2)(\kappa_2+\kappa_3)(\kappa_3-\kappa_4)+2e^{2qd}(\kappa_2-\kappa_3)(\kappa_1\kappa_3-\kappa_2\kappa_4) + e^{4qd}(\kappa_1+\kappa_2)(\kappa_2+\kappa_3)(\kappa_3+\kappa_4) \tag{7g}$$

where $q = |\mathbf{q}|$ and d is the interlayer distance. The dynamical dielectric function of the TLS system is [26]

$$\epsilon(\mathbf{q},\omega) = \det\left|\hat{1} - \hat{V}(\mathbf{q})\hat{\Pi}^{0,R}(\mathbf{q},\omega)\right| \tag{8}$$

The dynamical dielectric function of the coupled i-th and j-th layer is given by

$$\epsilon_{ij}(\mathbf{q},\omega) = \epsilon_i(\mathbf{q},\omega)\epsilon_j(\mathbf{q},\omega) - \mathrm{v}_{ij}(\mathbf{q})\mathrm{v}_{ji}(\mathbf{q})\Pi_i^0(\mathbf{q},\omega)\Pi_j^0(\mathbf{q},\omega), \tag{9}$$

where the dynamical dielectric function of the i-th layer is

$$\epsilon_i(\mathbf{q},\omega) = 1 - v_{ii}(\mathbf{q})\Pi_i^0(\mathbf{q},\omega) \tag{10}$$

The silicene polarization function is [14, 17]

$$\Pi_s^0(\mathbf{q},\omega) = -\frac{1}{2}\lim_{\delta\to 0}\sum_{\substack{\sigma,\xi,\\ \lambda,\lambda'=\pm 1}}\int_{R^2}\frac{dk_x dk_y}{4\pi^2}\left[1+\lambda\lambda'\frac{\hbar^2\mathrm{v}_F^2\mathbf{k}(\mathbf{k}+\mathbf{q})+\Delta_{\sigma\xi}^2}{E_{\sigma\xi}^{\lambda}(\mathbf{k})E_{\sigma\xi}^{\lambda'}(\mathbf{k}+\mathbf{q})}\right] \frac{n_F(E_{\sigma\xi}^{\lambda}(\mathbf{k})) - n_F(E_{\sigma\xi}^{\lambda'}(\mathbf{k}+\mathbf{q}))}{\hbar\omega + E_{\sigma\xi}^{\lambda'}(\mathbf{k}+\mathbf{q}) - E_{\sigma\xi}^{\lambda}(\mathbf{k}) + \mathrm{i}\delta}, \tag{11}$$

where $\xi = \pm 1$ distinguishes between inequivalent valleys K ($K^{'}$) and σ is the spin of the electron. Also $\Delta_{\sigma\xi} = |\sigma\xi\Delta_{SO} - \Delta_z|$ where Δ_{SO} is the spin-orbit coupling and Δ_z is the on-site potential difference caused by the asymmetry between A and B sublattices when an out of plane electric field is applied. The energy spectrum is $E^{\lambda}_{\sigma\xi}(\mathbf{k}) = \lambda\sqrt{\hbar^2 \mathrm{v}_F^2|\mathbf{k}|^2 + \Delta^2_{\sigma\xi}}$ where $\lambda = \pm 1$. From now on we assume that Δ_{SO}= 3.9 meV and $\Delta_z = 0.75\Delta_{SO}$. The silicene Fermi energy is E_F and the silicene Fermi velocity is v_F. In the regime $\hbar v_F q \ll \hbar\omega \ll E_F$, Eq. (11) reduces [17] to

$$\Pi^0_s(\mathbf{q},\omega) \approx \sum_{\xi,\sigma=\pm 1} \frac{E_F}{4\pi\hbar^2}\frac{q^2}{\omega^2}\left[1 - \left(\frac{\Delta_{\xi,\sigma}}{E_F}\right)^2\right]\Theta(E_F - \Delta_{\xi,\sigma}) \tag{12}$$

The carrier density n_e in silicene is linked to E_F through the following formula [18]

$$E_F = \sqrt{\pi\hbar^2 v_F^2 n_e + \frac{1}{2}(\Delta^2_{>} + \Delta^2_{<})}, \tag{13}$$

where $\Delta_{>} = |\Delta_{SO} + \Delta_z|$ and $\Delta_{<} = |\Delta_{SO} - \Delta_z|$.

In this paper we are interested in studying the plasmonic spectral weight. The first step is to determine the plasmonic branches from the zeroes of dynamical dielectric function of the TLS system with the help of Eq. (8)

$$\epsilon(\mathbf{q}, \omega_{pl} - \mathrm{i}\gamma_{pl}) = 0 \tag{14}$$

The plasmon branch is given by $\omega_{pl} \equiv \omega_{pl}(\mathbf{q})$ and the decay rate is given by $\gamma_{pl} \equiv \gamma_{pl}(\mathbf{q})$. We work under the assumption of weak damping ($\gamma_{pl} \ll \omega_{pl}$) which throughout the paper it will mean $\gamma_{pl}/\omega_{pl} \leq 0.1 \ll 1$. Therefore the plasmon branches and decay rate will be determined with the help of the following equations [26]

$$\mathrm{Re}\ \epsilon(\mathbf{q}, \omega_{pl}) = 0 \tag{15}$$

and

$$\gamma_{pl} = \mathrm{Im}\ \epsilon(\mathbf{q}, \omega_{pl}) \left[\left.\frac{\partial \mathrm{Re}\ \epsilon(\mathbf{q},\omega)}{\partial\omega}\right|_{\omega=\omega_{pl}}\right]^{-1} \tag{16}$$

The second step is to study the behavior of the loss function because it provides the total spectral weight associated with the plasmonic branches [24, 25]. Its expression is

$$-\mathrm{Im}\ \mathrm{Tr}[\hat{\Pi}^R(\mathbf{q},\omega)] = \\ -\mathrm{Im}\left[\frac{\Pi^0_1(\mathbf{q},\omega)\epsilon_{23}(\mathbf{q},\omega) + \Pi^0_2(\mathbf{q},\omega)\epsilon_{13}(\mathbf{q},\omega) + \Pi^0_3(\mathbf{q},\omega)\epsilon_{12}(\mathbf{q},\omega)}{\epsilon(\mathbf{q},\omega)}\right]. \tag{17}$$

When the loss function is restricted to the undamped part of a plasmon branch it

reduces to

$$-\frac{1}{\pi}\text{Im Tr}[\hat{\Pi}^R(\mathbf{q},\omega)]\Big|_{pl} = \text{Re}\left[\Pi_1^0(\mathbf{q},\omega)\epsilon_{23}(\mathbf{q},\omega)+\Pi_2^0(\mathbf{q},\omega)\epsilon_{13}(\mathbf{q},\omega)+\right.$$
$$\left.\Pi_3^0(\mathbf{q},\omega)\epsilon_{12}(\mathbf{q},\omega)\right]\left[\frac{\partial \text{Re}\,\epsilon(\mathbf{q},\omega)}{\partial\omega}\Big|_{\omega=\omega_{pl}}\right]^{-1}\delta(\omega-\omega_{pl}). \quad (18)$$

From now on we set $\Pi_i^0(\mathbf{q},\omega)\equiv\Pi_s^0(\mathbf{q},\omega)$ for $i\in\{1,2,3\}$ and we will use the following adimensional variables $\bar{q}\equiv\hbar v_F q/E_F$, $\bar{\omega}\equiv\hbar\omega/E_F$, $\bar{\Delta}_{\sigma\xi}=\Delta_{\sigma\xi}/E_F$, $\bar{d}\equiv(E_F/\hbar v_F)d$, $\bar{\gamma}_{pl}\equiv\hbar\gamma_{pl}/E_F$ and $\alpha=e^2/4\pi\epsilon_0\hbar v_F\approx 4.4$.

3. RESULTS AND DISCUSSION

In the following subsections we will provide the numerical and analytical results for the frequency of plasmon oscillations and for the plasmonic spectral weight given by the loss function. We arrive at this results by determining the roots of Eq. (15). The lower frequency and higher frequency solutions relate to the out of phase and in phase oscillations of the carrier densities of the silicene layers. They are named acoustic (AC) plasmons $\bar{\omega}_{ac}(\bar{q})$ and optical (OP) plasmons $\bar{\omega}_{op}(\bar{q})$.

3.1. HOMOGENEOUS CASE

In the homogeneous case we let $\kappa_1=\kappa_2=\kappa_3=\kappa_4$. We let $\kappa_1=\kappa_{\text{SiO}_2}$ = 3.8. We plug Eq. (12) into Eq. (15) and for the resulting equation we find its roots. To leading order in $\bar{q}\to 0$ the plasmon branches are

$$\bar{\omega}_{ac,1}(\bar{q}\to 0)\approx\left(\frac{\bar{d}\alpha\sum\limits_{\xi,\sigma=\pm1}\left(1-\bar{\Delta}_{\xi,\sigma}^2\right)\Theta(1-\bar{\Delta}_{\xi,\sigma})}{3\kappa_1}\right)^{\frac{1}{2}}\bar{q} \quad (19a)$$

$$\bar{\omega}_{ac,2}(\bar{q}\to 0)\approx\left(\frac{\bar{d}\alpha\sum\limits_{\xi,\sigma=\pm1}\left(1-\bar{\Delta}_{\xi,\sigma}^2\right)\Theta(1-\bar{\Delta}_{\xi,\sigma})}{\kappa_1}\right)^{\frac{1}{2}}\bar{q} \quad (19b)$$

$$\bar{\omega}_{op}(\bar{q}\to 0)\approx\left(\frac{3\bar{q}\alpha\sum\limits_{\xi,\sigma=\pm1}\left(1-\bar{\Delta}_{\xi,\sigma}^2\right)\Theta(1-\bar{\Delta}_{\xi,\sigma})}{2\kappa_1}\right)^{\frac{1}{2}} \quad (19c)$$

We see that $\bar{\omega}_{ac,1}(\bar{q}\to 0)$, $\bar{\omega}_{ac,2}(\bar{q}\to 0)\sim\bar{q}$ and $\bar{\omega}_{op}(\bar{q}\to 0)\sim\bar{q}^{\frac{1}{2}}$ therefore displaying a similar $\bar{q}$-dependence as in the case of double layer systems [22, 23] and a three layer graphene (TLG) structure [20]. The differences between the TLS and the mentioned systems is given by the dependence of the TLS system on the band gap $\Delta_{\sigma\xi}$.

The analytical formulas for the the loss function restricted to the undamped plasmons, to leading order in $\bar{q}\to 0$, are obtained by plugging Eq. (12), Eq. (19a) for the first acoustic branch, Eq. (19b) for the second acoustic branch and Eq. (19c) for the optical branch into Eq. (18)

$$-\text{Im Tr}[\hat{\Pi}^R(\bar{q},\bar{\omega})]\Big|_{\bar{\omega}=\bar{\omega}_{ac,1}(\bar{q}\to 0)}\approx\frac{3\pi\kappa_1}{4\bar{d}}\bar{\omega}_{ac,1}(\bar{q}\to 0) \tag{20a}$$

$$-\text{Im Tr}[\hat{\Pi}^R(\bar{q},\bar{\omega})]\Big|_{\bar{\omega}=\bar{\omega}_{ac,2}(\bar{q}\to 0)}\approx\frac{\pi\kappa_1}{4\bar{d}}\bar{\omega}_{ac,2}(\bar{q}\to 0) \tag{20b}$$

$$-\text{Im Tr}[\hat{\Pi}^R(\bar{q},\bar{\omega})]\Big|_{\bar{\omega}=\bar{\omega}_{op}(\bar{q}\to 0)}\approx\frac{\pi\kappa_1}{6}\bar{\omega}_{op}(\bar{q}\to 0)\bar{q} \tag{20c}$$

These formulas are the same as the formulas from the TLG structure with the caveat that the plasmon frequencies display the dependence on the band gap $\Delta_{\sigma\xi}$ in the TLS system.

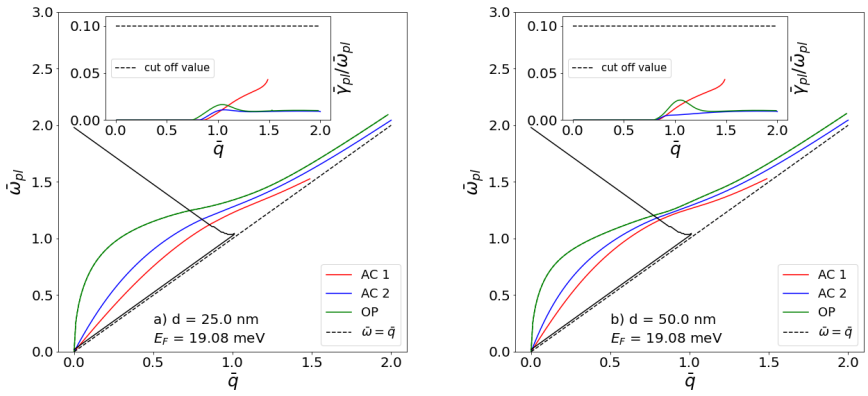

Fig. 2 – Frequency of AC 1, AC 2 and OP plasmons in the homogeneous TLS system for fixed carrier density $n_e = 10^{11}$ cm^{-2} and varying inter-layer distances (a) d = 25 nm, (b) d = 50 nm. The insets from Figs. 2(a) - (b) display the ratio $\bar{\gamma}_{pl}/\bar{\omega}_{pl}$ that quantifies the weak damping assumption for a fixed cut-off value. The solid black curve bounds the region where Im $\epsilon(\bar{q},\bar{\omega})=0$.

As in the case of the TLG system, the loss function in the long wavelength limit restricted to the two undamped AC plasmon branches behaves as $-\text{Im Tr}[\hat{\Pi}^R(\bar{\mathbf{q}},\bar{\omega}_{ac}(\bar{q}\to 0))]\sim\bar{q}$ while its restriction to the undamped OP plasmon displays a behavior

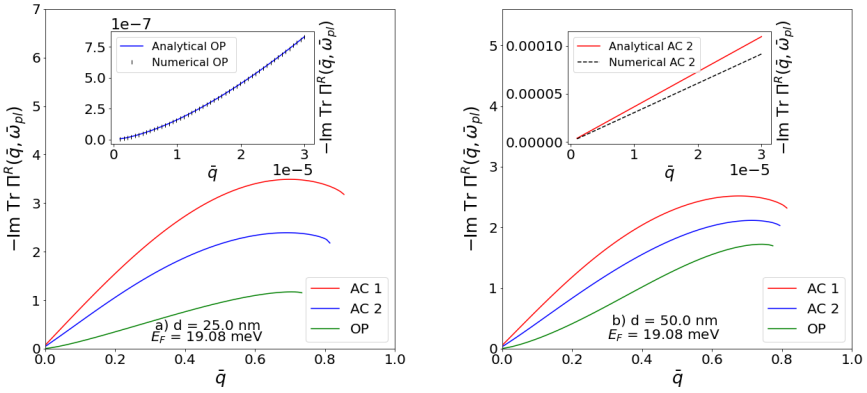

Fig. 3 – -Im Tr$[\hat{\Pi}^R(\bar{q},\bar{\omega}_{pl})]$ of undamped AC 1, AC 2 and OP plasmons in the homogeneous TLS system for fixed carrier density $n_e = 10^{11}$ cm^{-2}, varying inter-layer distances (a) d = 25 nm, (b) d = 50 nm. The insets from Figs. 3(a) - (b) display the numerical evaluation of Eq. (18) in the $\bar{q} \to 0$ limit versus the analytical formulas from Eqs. $(20a) - (20c)$.

$-\mathrm{Im\ Tr}[\hat{\Pi}^R(\bar{\mathbf{q}},\bar{\omega}_{op}(\bar{q} \to 0))] \sim \bar{q}^{\frac{3}{2}}$. Evaluating numerically Eqs. (20a)-(20c) we can see that the two undamped AC plasmon branches carry more spectral weight than the undamped OP plasmon branch in the limit $\bar{q} \to 0$.

Figures 2(a)-(b) show the AC and OP plasmon curves in the homogeneous case for different interlayer distances d. We use the assumption of weak damping, that is to say that we define a cut-off value such that $\bar{\gamma}_{pl}/\bar{\omega}_{pl} \leq 0.1$. For $\bar{\gamma}_{pl}/\bar{\omega}_{pl} \leq 0.1$ we obtain the physical frequencies of the plasmon branch while for $\bar{\gamma}_{pl}/\bar{\omega}_{pl} > 0.1$ we get the nonphysical frequencies of the plasmon branch. We observe that the condition $\bar{\gamma}_{pl}/\bar{\omega}_{pl} \leq 0.1$ is fulfilled for all the computed plasmon frequencies while in TLG system this does not happen. We can see that at the point q_c, where the plasmon curves pass the upper boundary (solid black curve) of the region where Im $\epsilon(\bar{q},\bar{\omega}) = 0$, the branches come very close as we increase the interlayer distance. A similar behavior is observed also in double layer graphene (DLG) system [22] and in the TLG system [20].

Figures 3(a)-(b) illustrate the behavior of the loss function restricted to the three branches of the undamped plasmons. We observe a similar qualitative behavior as in the case of the TLG system. We first observe that the spectral weight associated with the two acoustic plasmon branches dominates over that of the optical plasmon branch. This generalizes the results from the limit $\bar{q} \to 0$. We can see that there is that a domination in reverse order, meaning that the spectral weight associated with the first acoustic branch dominates over that of the second acoustic branch which in turn dominates over the spectral weight of the optical branch. We observe that the spectral

weights tend to close on each other as interlayer distance is varied from d = 25 to d = 50 nm.

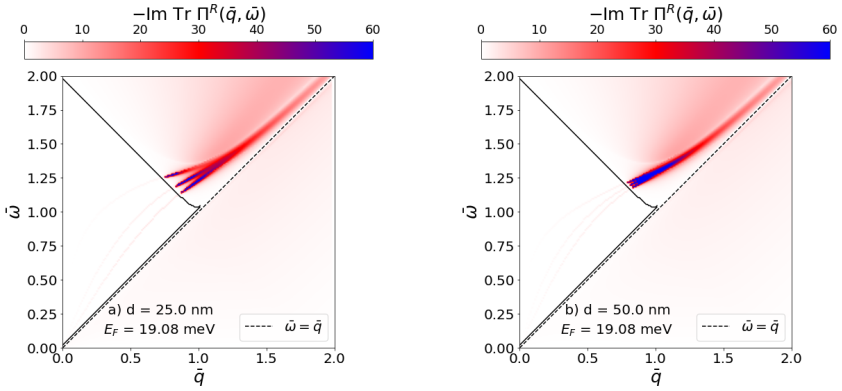

Fig. 4 – -Im Tr$[\hat{\Pi}^R(\bar{q},\bar{\omega})]$ in the $(\bar{q},\bar{\omega})$ plane for the homogeneous TLS system with fixed carrier density $n_e = 10^{11}$ cm^{-2} and varying inter-layer distances (a) d = 25 nm, (b) d = 50 nm. The solid black curve bounds the region where Im $\epsilon(\bar{q},\bar{\omega}) = 0$.

Figures 4(a)-(b) illustrate the damped plasmons which are related to a broadened peak in the loss function. For large broadening the plasmon becomes overdamped and there is no associated peak in the loss function. We can observe that for the case when the interlayer distance is d = 25 nm the broadened peaks from the three branches can be distinguished while for the case when the interlayer distance is d = 50 nm those contributions cannot be distinguished. This means that the spectral weights of the three plasmon branches start to merge as we increase the interlayer distance. A similar behavior happens in the TLG system as well.

3.2. INHOMOGENEOUS CASE

In the inhomogeneous case we set $\kappa_1 = \kappa_{SiO_2}$ = 3.8, $\kappa_2 = \kappa_{SiO_2}$ = 3.8, $\kappa_3 = \kappa_{Al_2O_3}$ = 9.1 and $\kappa_4 = \kappa_{Air} = 1$.

Figures 5(a)-(b) show the plasmon frequencies in the inhomogeneous case. We can observe that they display a similar behavior with those in the homogeneous case.

Figures 6(a)-(b) display the behavior of the loss function restricted to the three branches of the undamped plasmons. We observe similar behaviors to the ones in the homogeneous case. We can can see that the spectral weights of the two acoustic plasmon branches dominate over the spectral weight of the optical plasmon. We also observe that the spectral weights tend to approach one another as we increase the interlayer distance.

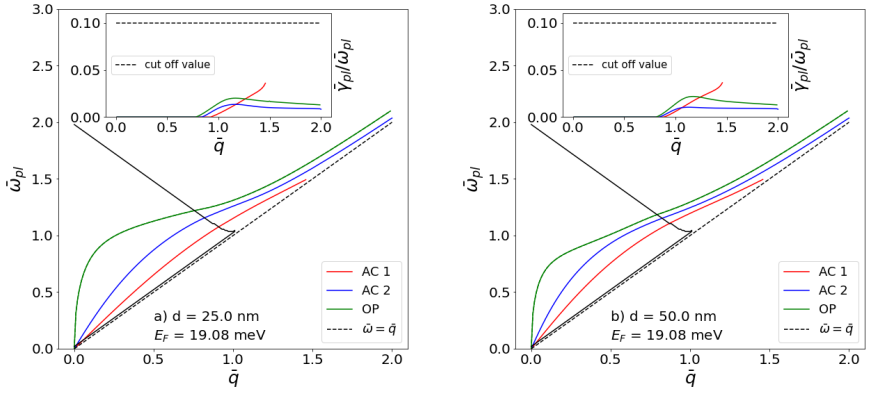

Fig. 5 – Frequency of AC 1, AC 2 and OP plasmons in the inhomogeneous TLS system for a fixed carrier density $n_e = 10^{11}$ cm^{-2}, varying inter-layer distances (a) $d = 25$ nm, (b) $d = 50$ nm. The insets from Figs. 5(a) - (b) display the ratio $\bar{\gamma}_{pl}/\bar{\omega}_{pl}$ that quantifies the weak damping assumption for a fixed cut-off value. The solid black curve bounds the region where Im $\epsilon(\bar{q}, \bar{\omega}) = 0$

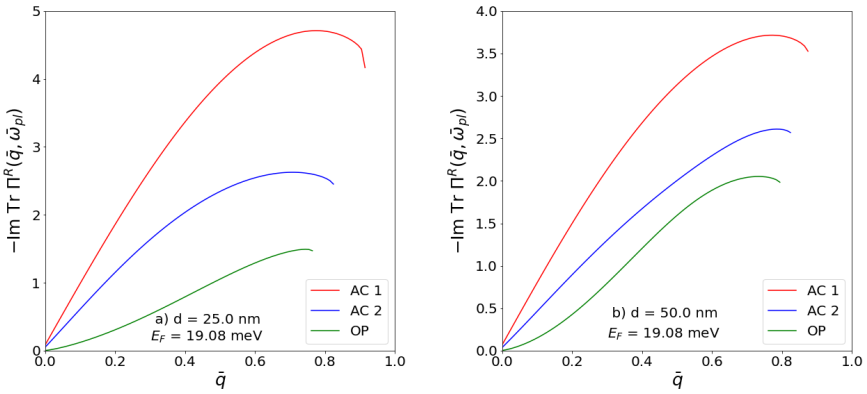

Fig. 6 – $-\mathrm{Im\ Tr}[\hat{\Pi}^R(\bar{q}, \bar{\omega}_{pl})]$ of undamped AC 1, AC 2 and OP plasmons in the inhomogeneous TLS system fixed carrier density $n_e = 10^{11}$ cm^{-2}, varying inter-layer distances (a) $d = 25$ nm, (b) $d = 50$ nm.

Figures 7(a)-(b) illustrate the damped plasmons in the inhomogeneous case. Contrary to the homogeneous case we can observe that for $d = 25$ nm and $d = 50$ nm the spectral weights of the three branches can be distinguished. The effect of the inhomogeneity appears at $d = 50$ nm because we can still distinguish the contributions from the three branches which in the homogeneous case does not happen. A similar behavior we can observe also in the TLG system.

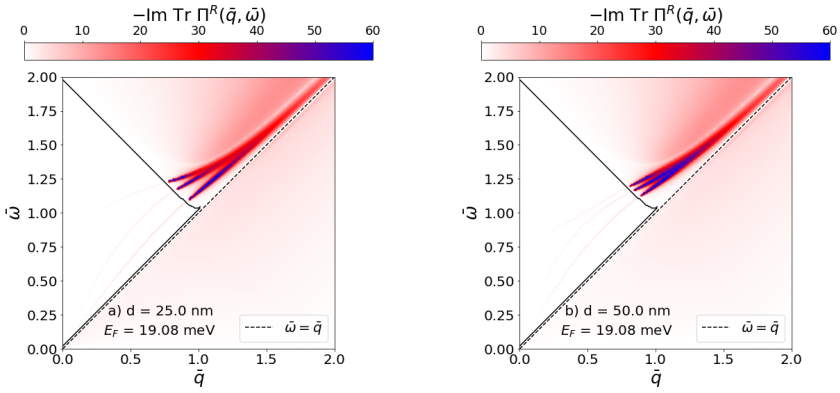

Fig. 7 – $-\text{Im Tr}[\hat{\Pi}^R(\bar{q},\bar{\omega})]$ in $(\bar{q},\bar{\omega})$ in the inhomogeneous TLS system fixed carrier density $n_e = 10^{11}$ cm^{-2}, varying inter-layer distances (a) $d = 25$ nm, (b) $d = 50$ nm. The solid black curve bounds the region where Im $\epsilon(\bar{q},\bar{\omega}) = 0$.

4. CONCLUSIONS

Summing up, we compute for the homogeneous and inhomogeneous cases the frequencies of the plasmon oscillations and the loss function in a TLS system at zero temperature using the RPA approximation. In the homogeneous case, in the $\bar{q} \to 0$ limit, when the loss function is restricted to the acoustic and optical plasmons, we observe a behavior of the type $-\text{Im Tr}[\hat{\Pi}^R(\bar{q},\bar{\omega}_{ac,1}(\bar{q} \to 0))] \sim \bar{q}$, $-\text{Im Tr}[\hat{\Pi}^R(\bar{q},\bar{\omega}_{ac,2}(\bar{q} \to 0))] \sim \bar{q}$ and $-\text{Im Tr}[\hat{\Pi}^R(\bar{q},\bar{\omega}_{op}(\bar{q} \to 0))] \sim \bar{q}^{\frac{3}{2}}$. This is similar to the TLG system. The spectral weight of loss function associated with the undamped plasmon branches is dominated by the acoustic plasmons. The spectral weights of the undamped plasmons start to approach one another as the interlayer distance is increased. Also we observe that in the $(\bar{q},\bar{\omega})$ plane as we start from well defined separated broadened peaks of the damped plasmon, as we increase the inter-layer distance, these peaks start to merge. Similar behaviors are observed also in the TLG system.

The only notable effect that the inhomogeneity produces is that it prevents the merging of the branches at the q_c point for $d = 50$ nm as it happens in the homogeneous case. Thus in the inhomogeneous case we are able to distinguish the contributions of the broadened peaks of the damped plasmons which in the homogeneous case is not possible.

REFERENCES

1. Z. Ni, Q. Liu, K. Tang, J. Zheng, J. Zhou, R. Qin, Z. Gao, D. Yu, J. Lu, Nano Letters **12**(1), 113 (2012).
2. N. Drummond, V. Zólyomi, V. Falko, Physical Review B **85** (7), 075423 (2012).
3. H.R. Chang, J. Zhou, H. Zhang, Y. Yao, Physical Review B **89** (20), 201411 (2014).
4. J. Zhao, H. Liu, Z. Yu, R. Quhe, Y. Wang, C.C. Liu, H. Zhong, N. Han, J. Lu, Y. Yao, K. Wu, Progress in Materials Science **83**, 24-151 (2016).
5. A. Grigorenko, M. Polini, K. Novoselov, Nature Photonics **6** (11), 749 (2012).
6. S. Xia, X. Zhai, L. Wang, S. Wen, Photonics Research **6** (7), 692 (2018).
7. S. Xia, X. Zhai, Y. Huang, J. Liu, L. Wang, S. Wen, Optics Letters **42** (15), 3052 (2017).
8. V. Ryzhii, M. Ryzhii, V. Mitin, M. S. Shur, A. Satou, T. Otsuji, Journal of Applied Physics **113** (17) (2013).
9. H. Nasari, M. S. Abrishamian, P. Berini, Optics Express **24** (1), 708 (2016).
10. Y. Li, Y. Su, X. Zhai, L. Wang, Europhysics Letters **125** (3), 34002 (2019).
11. F.H. Koppens, D.E. Chang, F.J. García de Abajo, Nano Letters **11** (8), 3370 (2011).
12. P. Avouris, M. Freitag, IEEE Journal of selected topics in quantum electronics **20** (1), 72 (2013).
13. B. Van Duppen, P. Vasilopoulos, F.M. Peeters, Physical Review B **90** (3), 035142 (2014).
14. C.J. Tabert, E.J. Nicol, Physical Review B **89** (19), 195410 (2014).
15. J.Y. Wu, S.C. Chen, M.F. Lin, New Journal of Physics **16** (12), 125002 (2014).
16. A. Iurov, G. Gumbs, D. Huang, Journal of Physics: Condensed Matter **29** (13), 135602 (2017).
17. N. Dadkhah, T. Vazifehshenas, M. Farmanbar, T. Salavati-Fard, Journal of Applied Physics **125** (10) (2019).
18. A. Iurov, G. Gumbs, D. Huang, G. Balakrishnan, Physical Review B **96** (24), 245403 (2017).
19. N. Van Men, Journal of Physics: Condensed Matter **34** (8), 085301 (2021).
20. C. Caraiani, L. Ion, V. Baran, *Loss function in a three layer graphene heterostructure at zero temperature*, submitted to Solid State Communications, 2024.
21. D.T.K. Phuong, N. Van Men, Physics Letters A **383** (33), 125971 (2019).
22. E.H. Hwang, S. Das Sarma, Physical Review B **80** (20), 205405 (2009).
23. N. Van Men, N.Q. Khanh, D.T.K. Phuong, Solid State Communications **294**, 43 (2019).
24. T. Stauber, G. Gómez-Santos, New Journal of Physics **14** (10), 105018 (2012).
25. T. Stauber, G. Gómez-Santos, Physical Review B **85** (7), 075410 (2012).
26. A. Fetter, J. Walecka, Quantum Theory of Many-particle Systems, Dover Books on Physics, Dover Publications, 2003.